Sequential Antifouling Surface for Efficient Modulation of the Nanoparticle-Cell Interactions in Protein-Rich Environments

Zhang, F.; Kong, L.; Liu, D.; Li, W.; Mäkilä, E.; Correia, A.; ... ; Santos, H.A.

ADVANCED THERAPEUTICS
www.advtherap.com

Sequential Antifouling Surface for Efficient Modulation of the Nanoparticle–Cell Interactions in Protein-Rich Environments

*Feng Zhang, Li Kong, Dongfei Liu, Wei Li, Ermei Mäkilä, Alexandra Correia, Rici Lindgren, Jarno Salonen, Jouni J. Hirvonen, Hongbo Zhang, Alexander Kros, and Hélder A. Santos**

Modulating the nanoparticle (NP)–cell interactions in protein-rich environments is of increasing significance to nanomedicine. One major challenge is that the synthetic identity (such as targeting) of NPs endowed for this purpose can be adversely altered by opsonization processes. The formed protein corona on NPs can cause fast clearance of NPs by macrophages and reduced cancer cell uptake. The transformable NPs, which are grafted with a cleavable antifouling surface to achieve inactive-active targeting form conversion, offer great promise to efficiently modulate NP–cell interactions. However, most of the transformable NPs lack a sustainable protection mechanism to avoid the influence of the protein corona during the post-transformation period, leading to the re-opsonization on NPs. Here, the authors design a smart transformable nanosystem with a photo-triggered zwitterion-induced sequential antifouling surface to efficiently reduce protein adsorption on NPs and modulate the NP–cell interactions in protein-rich environments. The authors demonstrate that the primary PEGylated antifouling surface could protect the NPs against uptake by macrophages. Furthermore, the photo-induced secondary zwitterionic antifouling surface is shown to preserve the targeting capacity of biotin-modified NPs during the post-transformation period in protein-rich environments. In contrast, the biotin-conjugated NPs without antifouling surfaces almost lost the targeting specificity in protein-rich environment.

1. Introduction

Engineering the surface of nanoparticles (NPs) to target the cancer cells is one of the most important aims of nanomedicine. In view of the various intrinsic physical and structural properties, numerous nanostructures have been developed as carriers for therapeutics to regulate their pharmacokinetics and bio-distribution by passive or active targeting.[1–3] However, this targeting capacity can be deprived by the fast opsonization process in physiological environments (*e.g.* blood, interstitial fluid, and cellular cytoplasm).[4–6] The serum and plasma proteins deposit on the surface of NPs and then form protein corona, which can physically mask the physicochemical properties of NPs (e.g., material, size, charge, shape, and surface functional group) and significantly alter the fate of NPs, leading to the loss of targeting specificity and fast uptake by macrophages.[7–10] Furthermore, suboptimal NPs accumulation mediated by the expression of relevant receptor in normal cells also leads to the off-target of NPs.[11,12]

To inhibit the influence of protein opsonization and off-target effect, as well as promote the specificity to cancer cells, many inactive–active form conversion strategies, such as uncaging, charge conversion, and conformation change, have been developed to modulate the NP–cell interactions in physiological environments.[13–18] In these system, the antifouling surfaces (such as PEGylated surface or zwitterionic surface) act as inactive form to minimize the protein adsorption, reduce

F. Zhang, Dr. D. Liu, Dr. W. Li, A. Correia, Prof. J. J. Hirvonen, Prof. H. A. Santos
Drug Research Program
Division of Pharmaceutical Chemistry and Technology
Faculty of Pharmacy
University of Helsinki
Helsinki, FI-00014, Finland
E-mail: helder.santos@helsinki.fi
Dr. D. Liu, Prof. H. A. Santos
Helsinki Institute of Life Science
University of Helsinki
FI-00014, Helsinki, Finland
L. Kong, Prof. A. Kros
Leiden Institute of Chemistry
Leiden University
P.O. Box 9052, 2300 RA, Leiden, The Netherlands
E. Mäkilä, R. Lindgren, Prof. J. Salonen
Laboratory of Industrial Physics
Department of Physics
University of Turku
FI-20014, Turku, Finland
Prof. H. Zhang
Department of Pharmaceutical Sciences Laboratory,
Turku Center for Biotechnology
Åbo Akademi University
FI-20520, Turku, Finland

The ORCID identification number(s) for the author(s) of this article can be found under https://doi.org/10.1002/adtp.201800013

DOI: 10.1002/adtp.201800013

the macrophages uptake, and prolong the systemic circulation of the NPs.[19–21] The NPs conversion can be achieved by cleaving the antifouling surface by endogenous signals (such as pH and enzymes) or exogenous signals (such as photo), to expose the internal targeting segments for cell recognition. However, most of these efforts neglected a protection mechanism to guarantee the efficient exposure of the targeting segments during the post-transformation period of NPs in the protein-rich environment. As a result, the ensuing re-opsonization occurs to the NPs, leading to the loss of targeting specificity for cancer cell uptake.[9,22,23]

Here, we introduce a sequential antifouling strategy to avoid the protein adsorption and guarantee the efficient inactive–active form conversion of NPs in protein-rich environment. To achieve direct and efficient artificial modulation, ultraviolet (UV) was selected as the trigger for the NPs transformation. This sequential antifouling surface was constructed by PEGylation of the polyethylenimine (PEI) surface via a photocleavable ortho-nitrobenzyl (*o*-NB) linker, with biotin conjugated as targeting molecules.[24–26] The *o*-NB alcohol derivatives have been widely used as crosslinkers to construct photodegradable biomaterials.[27–30] The *o*-NB-based crosslinkers can be cleaved rapidly using low-intensity UV light irradiation (1.3 mW cm^{-2}).[27] Moreover, the cleavage of *o*-NB-based crosslinkers can also be achieved by two-photon infrared (IR) excitation or NIR-UV upconversion, allowing for deeper tissue penetration and increasing biosafety as compared to UV light.[28,31] Thus, *o*-NB-based photodegradable systems have the potential to achieve noninvasive controlled drug release in deep tissue spatially and temporally. The NPs transformation was achieved by photo-irradiation, resulting in cleavage of the outer PEG layer and concomitant formation of carboxylic acids. The generated negative charged carboxyl groups together with the positive charged amine groups constructed the zwitterionic surface of the NPs. This photo-triggered zwitterization process on PEI was accompanied by the exposure of biotin, resulting in the inactive–active targeting conversion. We demonstrated that this inactive–active targeting transformable delivery system with sequential antifouling surface has efficient photo-induced multistage NP–cell interactions with different kinds of cells (MDA-MB-231 cells, NIH 3T3 fibroblasts, and RAW 267.4 macrophages) in protein-rich environment.

2. Results and Discussion

2.1. Fabrication and Characterization of the NPs

The synthesis of the photocleavable acrylates-*ortho*-nitrobenzyl-PEG_{5000} construct is outlined in Figure S1, Supporting Information. The $mPEG_{5000}$ for forming protective PEG corona and acrylate for further modification on NPs were added to the nitrobenzyl alcohol. Both ^1H NMR spectrum (Figures S2–S6, Supporting Information) and MALDI-TOF mass spectrum (Figures S7 and S8, Supporting Information) confirmed the chemical structures during the synthesis.

The undecylenic acid–modified, thermally hydrocarbonized porous silicon (UnTHCPSi) NPs were used as a delivery system because of the available surface sites for chemical grafting and porous structure for loading of various cargos.[32–34] The polycationic PEI was conjugated onto the surface of UnTHCPSi by carbodiimide-based coupling reaction. Next, the biotin-N-hydroxysuccinimide (NHS) ester was used for biotinylation. The unreacted amine groups of PEI were used for further processing into the PEGylated and zwitterionic surfaces. Thiolation was performed using Traut's reagent (2-iminothiolane hydrochloride) in order to introduce thiol groups required for subsequent conjugation of photocleavable PEG segment via a Thiol–Michael addition click reaction.[35] After PEGylation, the UnTHCPSi-biotin-PEG-modified NPs (i.e., UPBP NPs) with PEGylated surface were obtained. After UV photolysis (wavelength at 365 nm), the ester bond on the acrylates-*ortho*-nitrobenzyl segment was cleaved, followed by the cleavage of the PEG shield and the generation of a zwitterionic surface. These photolyzed UPBP NPs with a zwitterionic surface were called Un-Bio@ZwS NPs. The fabrication process of this nanosystem is shown in **Scheme 1**. Fourier transform infrared (FTIR) spectra were used to confirm the successful surface modification of UnTHCPSi NPs (Figure S9, Supporting Information).

The time-evolution kinetics of *ortho*-nitrobenzyl-PEG_{5000} photolysis was quantified by high-performance liquid chromatography (HPLC) traces (**Figure 1**A; Figure S10, Supporting Information). We observed that approximately 80% conversion was achieved within 5 min of irradiation. Next, the UV-irradiation time-related cell viability and UV-induced DNA damage were tested on MDA-MB-231 cells, NIH 3T3 fibroblast, and renal epithelial cells (Figure S11, Supporting Information). It was shown that a short UV-irradiation time (<5 min) did not cause significant DNA damage, and the DNA proliferation capacity of MDA-MB-231 cells and NIH 3T3 fibroblasts reached more than 90% after 48 h incubation. However, upon increasing irradiation time (20 min), DNA damage was observed in the tested cell lines as a function of incubation time. Therefore, a UV-irradiation time of 5 min was chosen for the following experiments.

The zeta (ζ)-potential and size were measured after each modification step of the nanoparticles (Figure 1B,C; Table S1, Supporting Information). Briefly, the surface charge reversed from negative (−34.7 mV) to positive (+38.9 mV) after PEIylation. Upon biotinylation, the ζ-potential was reduced to +32.1 mV. Thiolation only slightly reduced the ζ-potential, in accordance with former findings.[36] The ζ-potential decreased significantly to +5.1 mV upon PEGylation of the NPs, indicating that the positively charged surface was effectively shielded by the PEG_{5000} corona. Finally, the PEGylated surface was converted into a zwitterionic surface after UV irradiation, leading to the change of the ζ-potential to −3.7 mV. The change in hydrodynamic diameter of the NPs was also monitored. After PEI conjugation and PEGylation, the particle size increased by ca. 32 nm (from 159 to 191 nm) and 53 nm (from 198 to 251 nm), respectively. After photolysis, the size decreased by ca. 45 nm (from 251 to 206 nm). Transmission electron microscopy (TEM) images showed the structures of the different types of prepared NPs (Figure 1D). Briefly, after modification by PEI and PEG, the porous structure of the UnTHCPSi NPs was coated by the polymer layer and was not visible in UPBP NPs. After photolysis, as the PEG corona was removed, the porous structure reappeared.

The pH-dependent ζ-potential changes of the NPs with antifouling surface is shown in Figure 1E. The ζ-potential of both

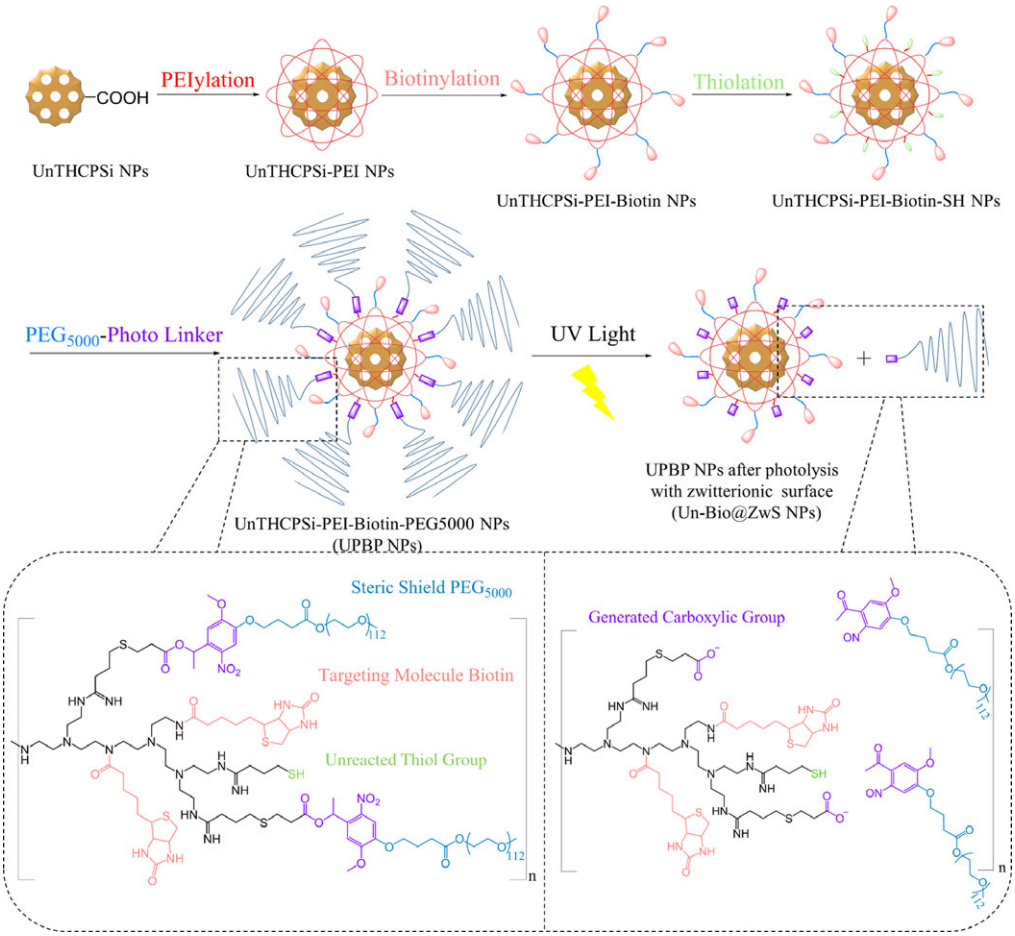

Scheme 1. Fabrication process of UPBP NPs and the relevant chemical structures before and after photolysis.

kinds of NPs increased by reducing the pH values of the dispersion medium from 8.0 to 5.0 in phosphate buffer solution (PBS, 0.01 M). However, the ζ-potential of the zwitterionic NPs featured a sharp transition from −12.4 mV to +17.2 mV. In contrast, the PEGylated NPs showed a slight transition of the ζ-potential within the range of pH values studied. The generated zwitterionic surface can maintain the surface charge close to neutral (from −3.7mV to +2.5mV) within pH value from 7.4 to 6.8, which are the typical pH value in normal tissue and malignant tissue, respectively. This property is favorable to reduce the biomolecule adsorption thermodynamically.[37]

2.2. NP—Protein Interaction Investigation and Colloidal Stability of NPs

Next, NP—protein interaction was investigated by the addition of 10% human serum to mimic the serum-rich environment.[9] In addition to the PEGylated and zwitterionic NPs, the UnTHCPSi-PEI-Biotin NPs (NPs without PEGylation) with cationic surface served as the control NPs in this experiment, because the cationic surface was prone to protein corona formation.[38] The amount of protein adsorption of UnTHCPSi-PEI-Biotin NPs was set as 100% in this comparison. As shown in Figures 1F and Figure S12, Supporting Information, both the PEGylated and zwitterionic NPs showed lower protein adsorption than the cationic NPs at pH 7.4 and pH 6.8. The colloidal stability of the UPBP NPs and Un-Bio@ZwS NPs were tested in HBSS buffer (1 × Hank's balanced salt solution, with 4-(2-hydroxyethyl)-1-piperazineethanesulfonic acid as buffering agent, pH = 7.4) and 10% human serum (Figure S13, Supporting Information). As a result of the weak surface charge of both NPs, aggregation was observed in HBSS buffer and human serum. However, the tendency of aggregation was attenuated over time, suggesting that the PEGylated and zwitterionic surfaces could maintain the colloid stability of the NPs. The colloidal stability also showed that the size of Un-Bio@ZwS was smaller than that of UPBP NPs in either protein-free or protein-rich environment.

2.3. Drug Loading Degree and Cumulative Drug Release Test

Based on the evaluation time of the photolysis-induced conversion of acrylates-*ortho*-nitrobenzyl-PEG_{5000}, it was expected that photolysis-induced transformation of NPs' surface (reduced PEG density) could lead to correspondingly photo-triggered drug

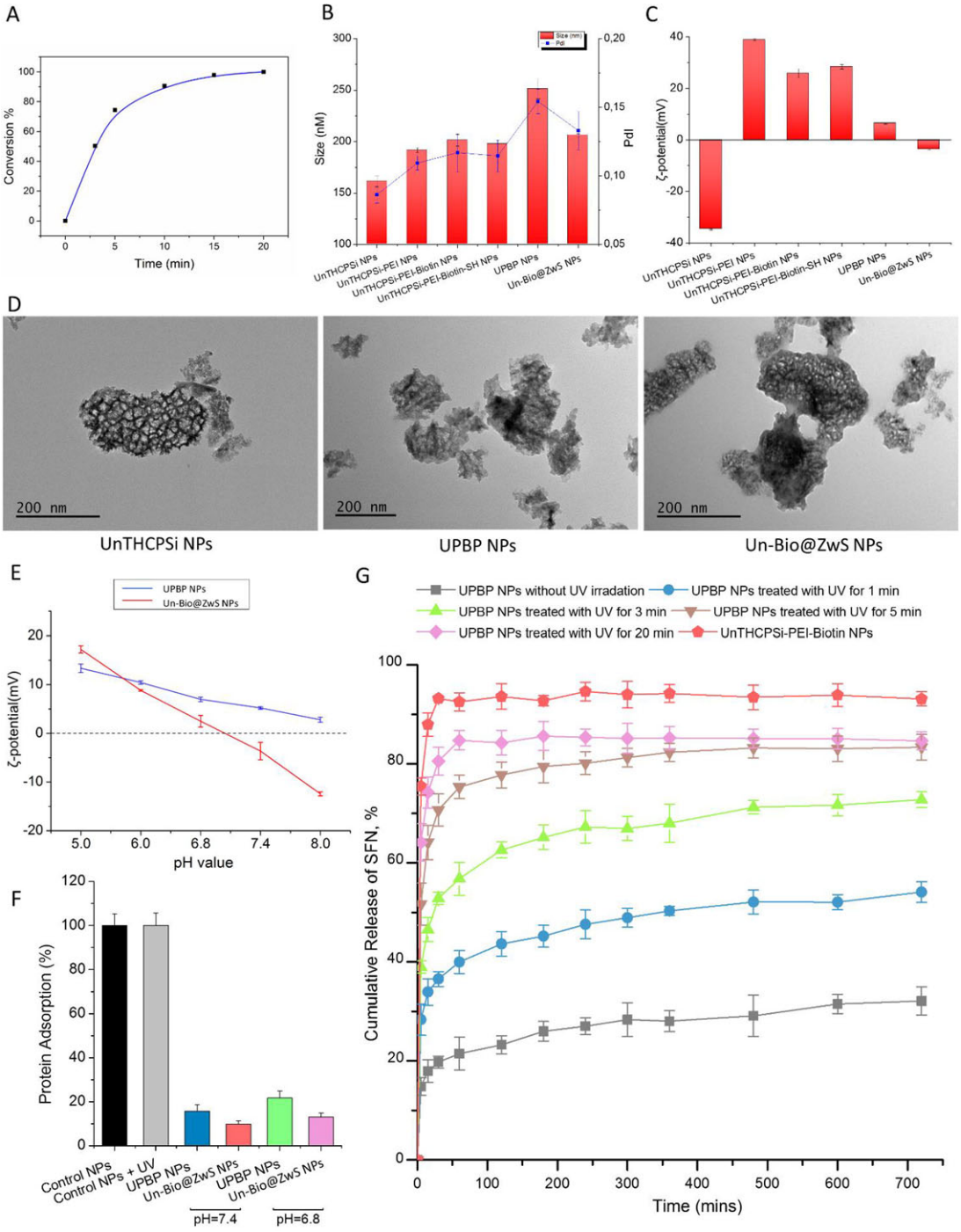

Figure 1. A) The time-evolution kinetics of acrylated-*ortho*-nitrobenzyl-PEG_{5000} photolysis (365 nm, 15–17 Mw cm^{-2}). B) Size and relevant polydispersibility index (PDI) of the prepared NPs. C) ζ-potential of the prepared NPs. D) TEM images of the obtained NPs. E) Influence of different pH values on the ζ-potential of NPs with PEGylated and zwitterionic surfaces. F) Human serum proteins adsorption onto the NPs after 1 h incubation at 37 °C, pH 7.4 or pH 6.8 (mean ± SD, $n = 3$). G) The cumulative release of SFN in 10% human serum.

release behavior. Firstly, the loading degree of a model anticancer drug, sorafenib (SFN), was tested by immersing the NPs in dimethyl sulfoxide (DMSO), reaching a drug loading of 23.7 ± 2.2% (mass ratio of SFN to NP). Then the drug release profiles of UPBP NPs undergone different UV-irradiation durations (0, 1, 3, 5, and 20 min, the relevant UV dose was 0, 0.97, 2.91, 4.85, and 19.40 J cm^{-2}) were determined in 10% human serum (Figure 1G). The UnTHCPSi-PEI-Biotin NPs served as a control. Due to the strong affinity between proteins and SFN molecules,[39] the amount of SFN released from UnTHCPSi-PEI-Biotin NPs was

as high as 75.5 ± 1.4% within 5 min, and reached a plateau at ca. 94% in 30 min. For UPBP NPs without UV photolysis, only ca. 35% of the payload was released after 12 h. The UV-irradiation duration significantly impacted the releasing profiles of SFN from the UPBP NPs. Specifically, the longer the UV-irradiation duration, the faster the release of SFN. The maximum amount of SFN released was significantly increased by increasing the UV-irradiation duration to 20 min. Using 5 min photolysis, ca. 75.3% of payloads was released from UPBP NPs in 1 h; the release profile reached a plateau at ca. 83% after 8 h. After 20 min of photolysis, the amount of drug released from UPBP NPs reached a plateau of ca. 85% in 1 h. It was noticed that the maximum amount of drug released from UPBP NPs after 20 min photolysis was less than that from UnTHCPSi-PEI-Biotin NPs (control). This lower level of release may be caused by the zwitterionic surface after photolysis, since the zwitterionic property could prevent the interaction of proteins with the drug and limit the drug release process.[40] The drug release profile from UPBP NPs following 5 min UV-exposing time in 10% human serum was measured for 2 h (Figure S14, Supporting Information).

2.4. Biocompatibility of the Prepared NPs

The cytotoxicity of the prepared NPs was evaluated using NIH 3T3 fibroblast (biotin-receptor negative cells) and MDA-MB-231 (biotin-receptor positive cells) cells at three time points (6, 24, and 48 h; **Figure 2**).[24,41] In addition to the aforementioned UPBP NPs and Un-Bio@ZwS NPs, the NPs without biotin modification (UnTHCPSi-PEI-PEG NPs and UnTHCPSi-PEI-PEG after photolysis, which are termed as UPP NPs and Un@ZwS NPs), were used as control groups to investigate the influence of the targeting molecules on the cytotoxicity.

Generally, the NPs with PEGylated surface (UPP and UPBP NPs) showed good biocompatibility to both cell lines. Especially at low concentrations (20 μg mL^{-1}), the cell viability was more than 95% after 48 h incubation. For the UPP and Un@ZwS NPs, the photolysis-induced NPs toxicity was observed by prolonging the incubation time and increasing the NPs concentration. The difference in the cytotoxicity between UPP and Un@ZwS NPs could be attributed to the shrinkage of particle size and the exposure of the thiolated surface after photolysis, which could enhance the cell internalization of NPs.[42–44] After modification with biotin, the cytotoxicity of Un-Bio@ZwS NPs was further increased, especially for MDA-MB-231 cells, suggesting that the active targeting segments could efficiently promote cell uptake of the NPs. For NIH 3T3 fibroblast cells that treated with Un-Bio@ZwS NPs, reduced cell viability was also observed after 48 h incubation, suggesting that the limited number of biotin receptors could still promote the endocytosis process of the NPs.

2.5. The Effect of Surface Properties and Environmental Conditions on Cell Uptake of NPs

To further study the effect of surface properties and environmental conditions on cell uptake of NPs, flow cytometry was used to quantitatively determine the amount of internalized NPs in both HBSS buffer and 10% human serum. In addition to the aforementioned NPs, the positive-charged UnTHCPSi-PEI-Biotin NPs served as a positive control to evaluate the cell uptake efficiency of NPs without antifouling surface in serum-free/serum-rich environment. The NPs were labeled with fluorescein isothiocyanate (FITC) for tracking. All the tested cell samples were treated with trypan blue to quench the outer fluorescence signal before cell sorting. The net fluorescence intensity (NFI) was obtained by subtracting autofluorescence of untreated cells.

For the test in HBSS buffer (**Figure 3**A,B), the cell sorting data showed that the uptake efficiency of UnTHCPSi-PEI-Biotin and Un-Bio@ZwS NPs by both cell lines was significantly higher than of the other NPs. For MDA-MB-231 cells, the NFI of UnTHCPSi-PEI-Biotin and Un-Bio@ZwS NPs reached 1817 and 1051 (mean value of fluorescence intensity), respectively. As a result of the positive charged surface of UnTHCPSi-PEI-Biotin NPs, their NFI was ≈1.7 times of Un-Bio@ZwS NPs. For NIH 3T3 cells, this difference was even bigger. Due to the lack of the biotin receptors, NIH 3T3 cells showed less uptake of Un-Bio@ZwS NPs. The relevant NFI of UnTHCPSi-PEI-Biotin NPs was approximately three times that of Un-Bio@ZwS NPs. However, the NFI of Un-Bio@ZwS NPs was still higher than the rest of the groups with antifouling surface (UPP, Un@ZwS, and UPBP NPs), suggesting that the exposure of biotin segment could still facilitate the uptake of NPs in normal cells, resulting in the off-target delivery of NPs. For both cell clines, no significant difference in uptake efficiency between UPP NPs and UPBP NPs was observed, which meant that the PEG corona could efficiently block the active targeting system. In comparison with UPP NPs, the Un@ZwS NPs showed higher cell uptake efficiency. These observations are in accordance with our former assumption that the enhanced NPs' cytotoxicity was a result of the enhanced NPs' cell uptake.

For both cell lines, the NFI of the UnTHCPSi-PEI-Biotin NPs showed a drastic reduction in the presence of human serum (Figure 3C,D). The reduction degree reached ca. 90% for both cell lines, indicating that the active targeting system and positive charged surface were blocked by the protein corona. In contrast, the NFI reduction for the Un-Bio@ZwS NPs was only ca. 60% for both cell lines. Consequently, the cell uptake efficiency of Un-Bio@ZwS NPs surpassed that of UnTHCPSi-PEI-Biotin NPs with ≈2.3 times for MDA-MB-231 cells and ≈1.3 times for NIH 3T3 fibroblasts. The higher cell uptake of Un-Bio@ZwS NPs indicated the reduced protein adsorption by the zwitterionic surface, which could efficiently maintain the performance of active targeting ligands.

The confocal fluorescence imaging was also used for evaluating the cell internalization efficiency to different kinds of NPs in HBSS buffer and 10% human serum (Figure 3E,F). Three kinds of NPs were tested, including the UPBP, Un-Bio@ZwS, and UnTHCPSi-PEI-Biotin NPs. The confocal images showed that the cell internalization of the UPBP NPs in both cell lines was very limited either in HBSS buffer or human serum. For both the cell lines tested, significant internalization inhibition of UnTHCPSi-PEI-Biotin NPs was observed in human serum, indicating that the formation of protein corona could efficiently block the NP−cell interactions (e.g., specific interaction and electronic adsorption). The relatively high extent of the NP internalization of Un-Bio@ZwS NPs in human serum indicated that

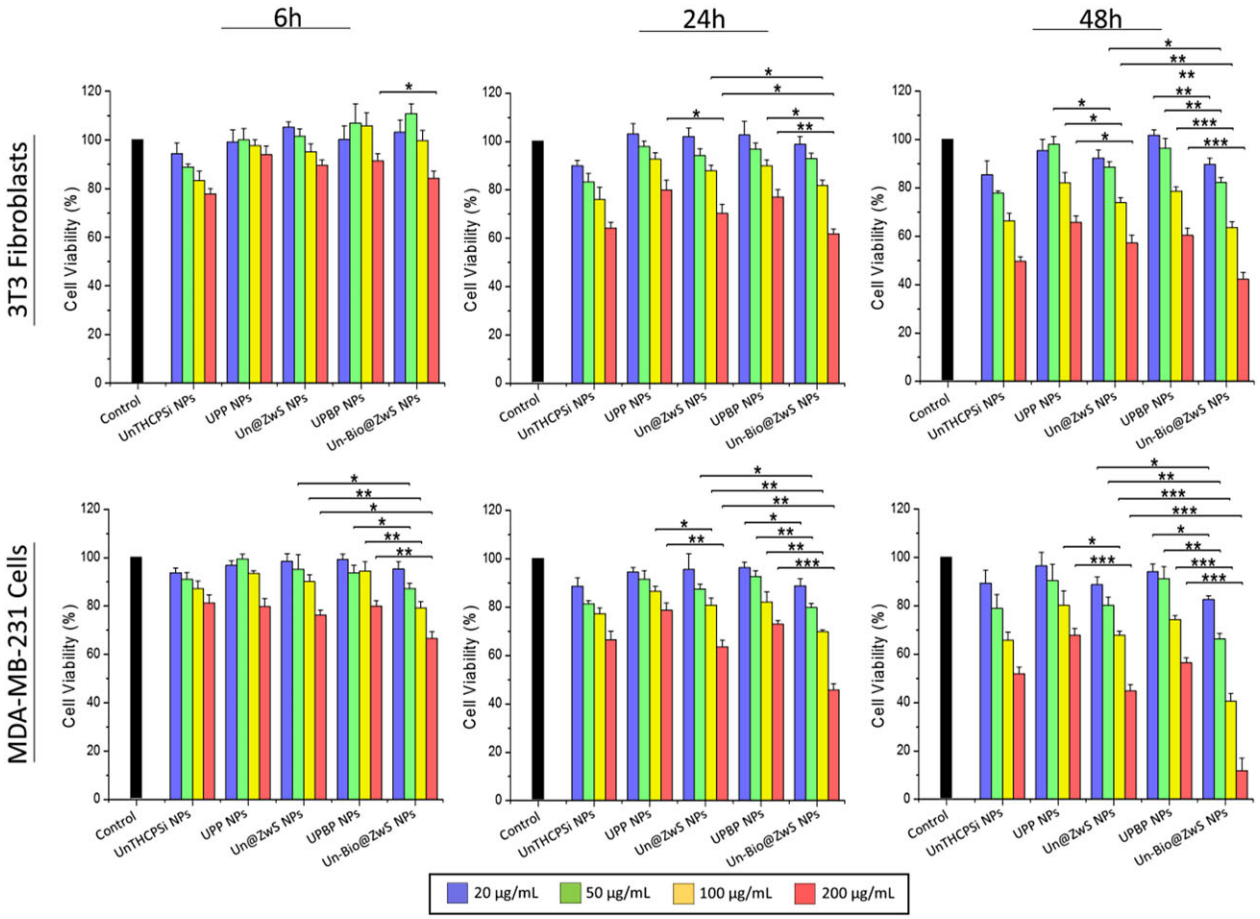

Figure 2. Cell viability of 3T3 fibroblast and MDA-MB-231 cells exposed to the different NPs assessed by the CellTiter-Glo Luminescent Assay after 6, 24, and 48 h of incubation. Four concentrations of NPs (20, 50, 100, and 200 μg mL^{-1}) were tested. Statistical analyses were made by one-way analysis of variance (ANOVA) with Bonferroni post-hoc test. The levels of significance were set at probabilities of $^{*}P < 0.05$, $^{**}P < 0.01$, and $^{***}P < 0.001$. Data are shown as mean ± S.D. ($n = 3$).

the specific targeting capacity was maintained on the zwitterionic surface.

2.6. The Effect of Surface Properties on NP—Macrophage Interactions

Next, RAW 267.4 macrophages were used to evaluate the possible macrophages clearance effect to the prepared NPs, by fluorescence-activated cell sorting in both HBSS buffer and 10% human serum (**Figure 4**A,B) and confocal fluorescence imaging (Figure 4C). For the NPs with antifouling surface, but without exposure of biotin (UPP, Un@ZwS, UPBP NPs), the macrophages showed limited internalization in serum-free/serum-rich environment, suggesting that the NPs with PEGylated or zwitterionic surface could efficiently avoid the macrophages' clearance. However, macrophages showed enhanced cell uptake to Un-Bio@ZwS NPs, compared with Un@ZwS NPs in serum-free/serum-rich environment. Unlike MDA-MB-231 cells and NIH 3T3 fibroblasts that showed sharp uptake reduction to UnTHCPSi-PEI-Biotin NPs after protein opsonization, the RAW 267.4 macrophage still showed the highest uptake efficiency to UnTHCPSi-PEI-Biotin NPs than the other NPs in 10% human serum, with only ca. 54% reduction of cell uptake compared with that in serum-free buffer. This phenomenon confirmed that the macrophages could efficiently capture the opsonized NPs, in view of the various overexpressed receptors for protein corona recognition.[45]

2.7. Antiproliferation Test of the Sorafenib-Loaded NPs

The drug (SFN) delivery efficiency of the UPBP system (SFN@UPBP NPs) was investigated in both HBSS buffer and 10% human serum using an antiproliferation test on MDA-MB-231 cells (**Figure 5**). The NPs transformation-induced cancer cell antiproliferation effect could be observed in both environments. This effect indicated that the PEGylated surface could improve the safety of NP-based formulation and restrict unexpected drug release. After photolysis, the NPs transformed into the active targeting form, thus promoting the cell internalization of NPs and enhancing the corresponding anticancer effect significantly.

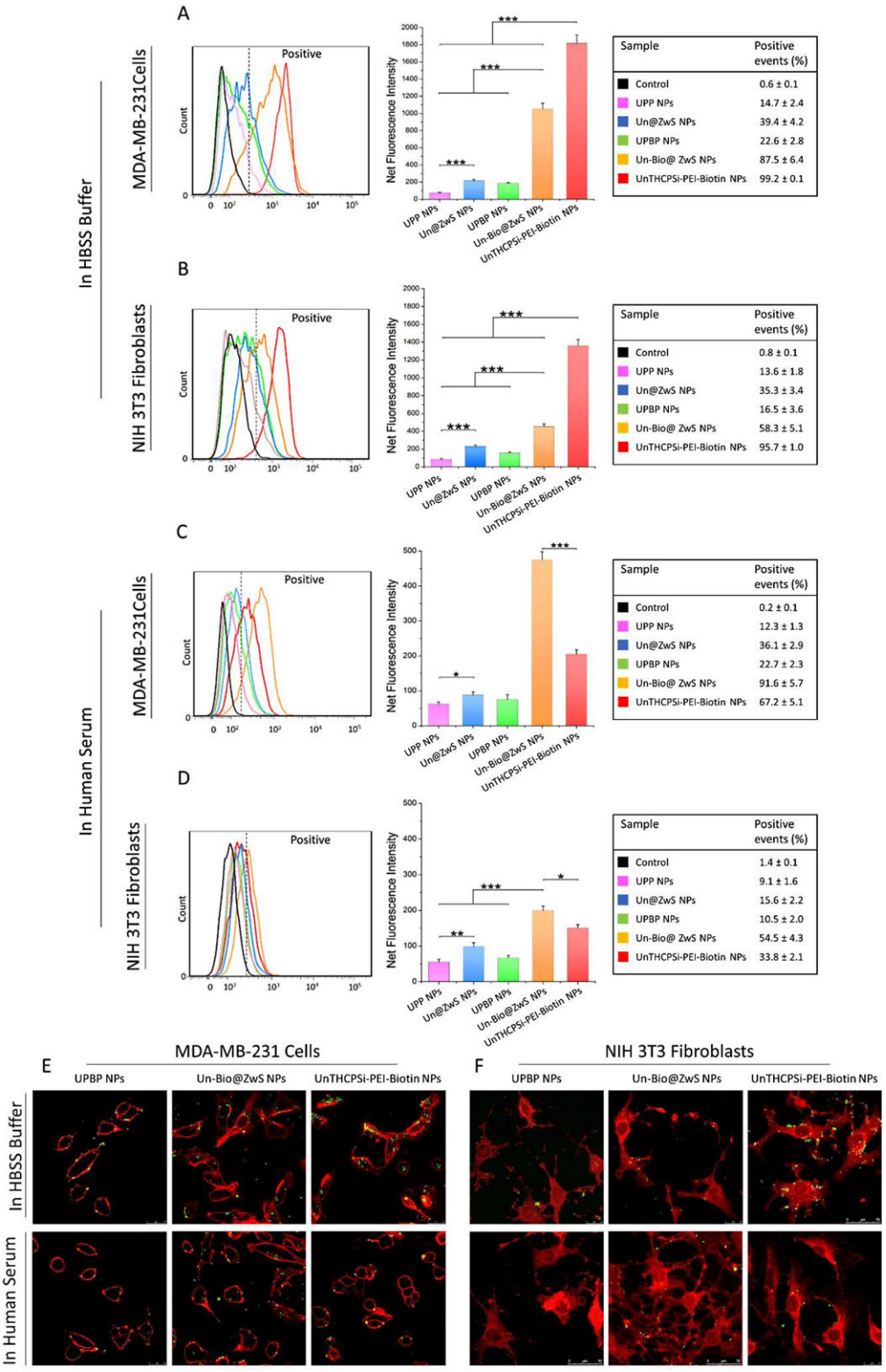

Figure 3. A–D) Flow cytometry quantitative analysis of MDA-MB-231 cells and 3T3 fibroblast in HBSS buffer and human serum. The cells were incubated with the NPs for 6 h at 37 °C. Data are shown as mean ± SD ($n = 3$). The levels of significance were set at probabilities of $^{*}P < 0.05$, $^{**}P < 0.01$, and $^{***}P < 0.001$. Data are shown as mean ± SD ($n = 3$). E) and F) Confocal fluorescence microscope images of MDA-MB-231 cells and 3T3 fibroblast treated with FITC-labeled NPs for 6 h at 37 °C (red: cell membranes stained with CellMask Deep Red; green: FITC-labeled NPs; yellow: co-localization of the NPs and the cell membrane).

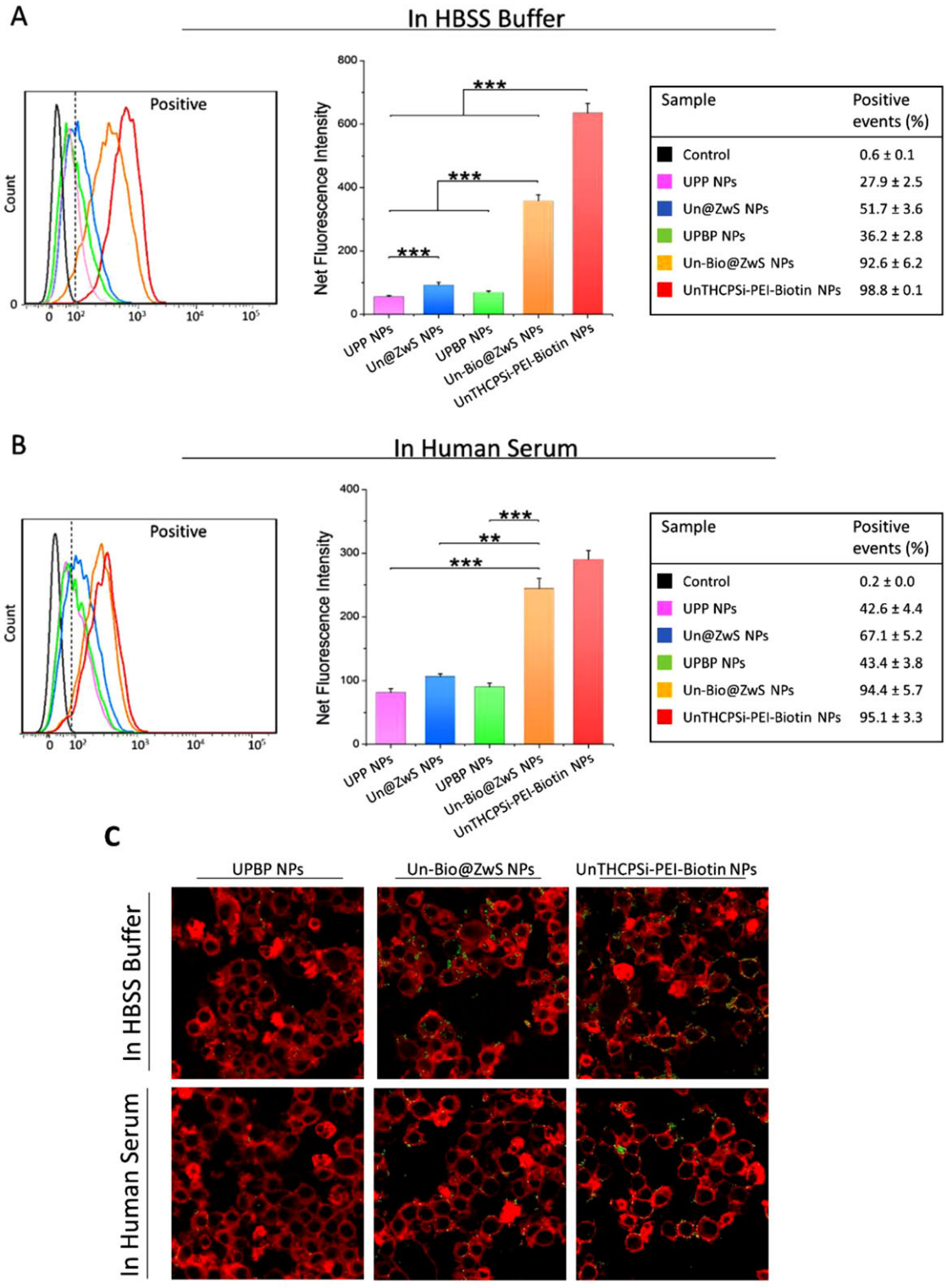

Figure 4. A) and B) Flow cytometry quantitative analysis of RAW 267.4 macrophages in HBSS buffer and human serum. The cells were incubated with the NPs for 6 h at 37 °C. Data are shown as mean ± SD ($n = 3$). The levels of significance were set at probabilities of $^{*}P < 0.05$, $^{**}P < 0.01$, and $^{***}P < 0.001$. Data are shown as mean ± SD ($n = 3$). C) Confocal fluorescence microscope images of RAW 267.4 macrophage cells treated with FITC-labeled NPs for 6 h at 37 °C (red: cell membranes stained with CellMask Deep Red; green: FITC-labeled NPs; yellow: co-localization of the NPs and the cell membrane).

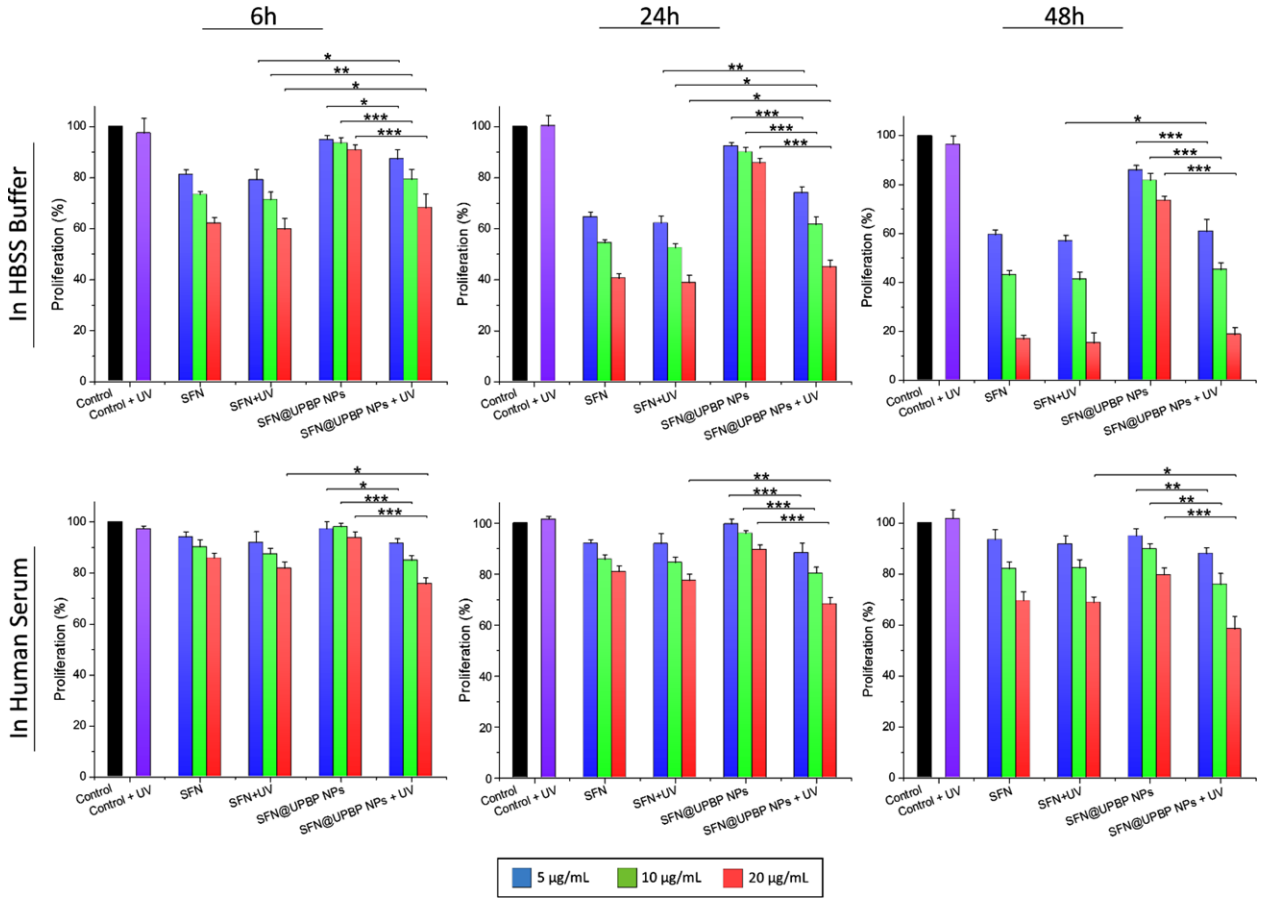

Figure 5. Cancer cell growth inhibition by treatment of MDA-MB-231 cells with free SFN and SFN-loaded UPBP NPs in HBSS buffer and human serum, with and without UV irradiation. Three different concentrations of the NPs (5, 10, and 20 μg mL^{-1}) were tested. The concentrations of the free drugs were based on the relevant drug loading degrees in the NPs. The MBA-MB-231 cells were exposed to the NPs for 6, 24, and 48 h at 37 °C. The levels of significance were set at probabilities of $^{*}P < 0.05$, $^{**}P < 0.01$, and $^{***}P < 0.001$. Data are shown as mean ± SD ($n = 3$).

For the comparison between free SFN and photolyzed SFN@UBPB NPs in HBSS buffer, as the cells directly espoused to SFN, free SFN exhibited a better therapeutic effect than SFN-loaded NPs. However, with prolonged incubation time, this difference was narrowed, and no significant differences between the groups of free drug and SFN-loaded NPs after 48 h incubation for concentrations of 10 and 20 μg mL^{-1} were observed. In human serum, as most of the SFN molecules form protein−drug complexes in serum-rich environment,[46] and as a result of the inefficient cell internalization to proteins,[47] the uptake of SFN decreased and the therapeutic effect of SFN was inhibited. However, compared with the free drug, SFN-loaded NPs at high concentration (20 μg mL^{-1}) showed higher cytotoxicity to cancer cells, indicating that the targeting traffic by NPs was more efficient in the delivery of SFN into the cells in the protein-rich environment.

3. Conclusion

We have successfully engineered a photo-triggered transformable system with sequential antifouling surface to better modulate the NP–cell interactions in protein-rich environment. This sequential antifouling surface can minimize the influence of opsonization during the whole transition process of NPs. In the in vitro assays with serum, we demonstrated that the PEGylated surface could effectively avoid the clearance from macrophages and unfavorable off-target effect. The secondary antifouling surface generated by photo-triggered zwitterization could preserve the targeting specificity of the NPs. It is expected that the photo switchable system can be further developed into a series of polycationic polymer-*o*-NB-based systems to achieve photo-triggered zwitterization for constructing sequential antifouling surface. Furthermore, to avoid the potential immunogenicity of PEG, the *o*-NB-based linker is also chemical achievable to graft other polymers to construct the primary antifouling surface, such as poly(carboxybetaine)[48] to obtain a better therapeutic performance. In addition, benefiting from the development of two-photon technology and NIR-UV upconversion technology, the photo-triggered zwitterization can be achieved in deep tissue and the DNA-damage caused by UV irradiation can be avoided. As a proof-of-concept, this study demonstrated that the transformable NPs with sequential antifouling surface may own great potential to improve the clinical performance of the drug delivery systems.

4. Experimental Section

Materials: All the chemical reagents were purchased with the highest grade available from Sigma Aldrich and used without further purification. Sorafenib (SFN) was purchased from LC laboratories (USA). Hank's balanced salt solution (10 × HBSS), Dulbecco's Modified Eagle's Medium (DMEM), Roswell Park Memorial Institute (RPMI), Dulbecco's phosphate buffer saline (10 × PBS), fetal bovine serum (FBS), trypsin (2.5%), nonessential amino acids (100 × NEAA), L-glutamine (200 mM), and penicillin-streptomycin (100 × PEST) were all purchased from HyClone (USA). Versene was purchased from Life Technologies (USA). Trypan blue was purchased from MP Biomedicals (Germany). The MDA-MB-231 breast carcinoma cells, NIH 3T3 fibroblasts, and RAW 267.4 macrophages were obtained from American Type Culture Collection.

Chemical Characterization: ^{1}H NMR spectra were measured on a Bruker AV-400MHz spectrometer. Chemical shifts were recorded in ppm. Tetramethylsilane (TMS) is used as an internal standard. Coupling constants are given in Hz. MALDI-TOF mass spectra were acquired using an Applied Biosystems Voyager System 6069 MALDI-TOF mass spectrometer. α-Cyano-4-hydroxycinnamic acid (CHCA) was used as matrix in all cases. Sample concentrations were ≈0.3 mg mL^{-1}.

The hydrodynamic size (z-average), polydispersity index (PdI), and ζ-potential distribution of the NPs were measured by Zetasizer Nano ZS (Malvern Instruments Ltd.). The relevant data were recorded as the average of three measurements.

The structure of the fabricated NPs was characterized by TEM under an acceleration voltage of 120 kV. The NPs samples were prepared by depositing them onto carbon-coated copper grids (300 mesh; Electron Microscopy Sciences, USA) and contrasting with 2% uranyl acetate solution. The NP-coated grids were dried at room temperature before the TEM imaging.

The surface chemical modifications were characterized using Fourier transform infrared spectroscopy (FTIR; Bruker Vertex 70). The KBr pellets were processed by mixing 300 μg of the samples with 200 mg of KBr (spectroscopy grade, Sigma-Aldrich, Finland). FTIR spectra were recorded from 3500 to 600 cm^{-1} with a resolution of 4 cm^{-1} at room temperature using OPUS 5.5 software.

Synthesis of the Photocleavable Acrylates-Ortho-*Nitrobenzyl-PEG$_{5000}$*: The synthesis of the photocleavable acrylates-*ortho*-nitrobenzyl-PEG$_{5000}$ is outlined in Figure S1, Supporting Information. The mPEG$_{5000}$ for forming protective PEG corona and acrylate for further modification on NPs were added to the nitrobenzyl alcohol. Both ^{1}H NMR spectrum (Figures S2–S6, Supporting Information) and MALDI-TOF mass spectrum (Figures S7 and S8, Supporting Information) confirmed the chemical structures during the synthesis. The detailed synthesis methods are listed in Supporting Information.

Preparation of UnTHCPSi NPs: The preparation of UnTHCPSi NPs was done via electrochemical anodization, as described in detail elsewhere.[49]

Fabrication of the Photo-Triggered Zwitterization-Induced Sequential Antifouling Surface on UnTHCPSi NPs: The UnTHCPSi NPs were firstly activated by carbodiimide chemistry based on N-hydroxysuccinimide (NHS) and 1-ethyl-3-(3-(dimethylamino)propyl)-carbodiimide (EDC). Briefly, 1 mg of UnTHCPSi NPs was activated by 10 μL of EDC for 20 min and then reacted with 2 mg of NHS in 1 mL of anhydrous dimethylformamide (DMF) for 24 h. The UnTHCPSi-NHS ester NPs were harvested by centrifugation (Sorvall RC 5B plus, Thermo Fisher Scientific, USA) at 13 000 × *g* for 5 min, washed three times with anhydrous DMF. The obtained UnTHCPSi-NHS ester NPs was then dispersed into 1 mL DMF with 10 mg polyethylenimine dissolved beforehand. After 12 h stirring, the obtained UnTHCPSi-PEI NPs were harvested by the aforementioned procedures.

One milligram of UnTHCPSi-PEI NPs was suspended in 1 mL of anhydrous DMF, then 10 μg of Biotin-NHS ester was added into the suspension. After 12 h stirring, the obtained UnTHCPSi-PEI-Biotin NPs were harvested by the aforementioned procedures.

The thiolation of the UnTHCPSi-PEI-Biotin NPs was operated under Ar atmosphere. One milligram of NPs was dispersed in 1 mL of phosphate buffer saline (PBS, pH 7.4, 0.01 M) and then the Traut's reagent was added (10 mg, 0.073 mmol). After 2 h, the NPs were harvested by centrifugation at 13 000 × *g* for 5 min, and washed by PBS (pH 7.4, 0.01 M) three times under Ar atmosphere. The obtained UnTHCPSi-PEI-Biotin-SH NPs was dispersed in PBS (pH 7.8, 0.01 M) with the concentration of 1 mg mL^{-1}.

Ten milligrams of the acrylates-*ortho*-nitrobenzyl-PEG$_{5000}$ (0.002 mmol) was added into the prepared UnTHCPSi-PEI-Biotin-SH NPs suspension. The mass ratio of the PEG to NPs was 10:1. The reaction was processed under Ar atmosphere for 24 h. The NPs was harvested by aforementioned method and then stocked in ethanol (99%) with Ar protection.

UV Irradiation: The UV-irradiation condition in this study was 365 nm and 15–17 mWcm^{-2}.

Time-Evolution of the Photolysis-Induced Conversion of the Acrylates-Ortho-*Nitrobenzyl-PEG$_{5000}$*: A solution of acrylates-*ortho*-nitrobenzyl-PEG$_{5000}$ (100 μM) in PBS was irradiated for 3 min, followed immediately by HPLC analysis. HPLC analysis was performed using a Shimadzu HPLC setup equipped with two LC-8A series pumps coupled to a Shimadzu ELSD-LT II detection system. Separation (Kinetex 5μ EVO, C18 100A, 150 × 4.6 mm, flow rate: 1 mL min^{-1}), in all instances, was carried out over a linear gradient of 10–95% B over 20 min with an initial 5 min hold at 10% B. HPLC mobile phases: A—H_2O (0.1% TFA); B—Acetonitrile (0.1% TFA). The same sample was then re-irradiated and this cycle was repeated for cumulative irradiation time points of 5, 10, 15, and 20 min. The conversion of compound was calculated by the peak area of start material in each trace.

Cell Culturing: The MDA-MB-231 breast cancer cells, NIH 3T3 fibroblasts, and RAW 267.4 macrophages were cultured in 75 cm^2 flasks (Corning Inc. Life Sciences, USA) in a standard BB 16 gas incubator (Heraeus Instruments GmbH, Germany) set at 95% humidity, 5% CO_2, and 37 °C. MDA-MB-231 cells were cultured in standard RPMI 1640 medium, NIH 3T3 fibroblasts and RAW 267.4 macrophages were cultured in DMEM medium, both supplemented with 10% v/v fetal bovine serum (FBS), 1% nonessential amino acids, 1% L-glutamine, penicillin (100 IU mL^{-1}), and streptomycin (100 mg mL^{-1}) (all from HyClone, USA). Cells' subculturing was conducted at 80% confluency, harvested prior to cell passaging and each experiment with trypsin—PBS—ethylenediaminetetraacetic acid.

UV-Induced DNA Damage: The detection of DNA damage by UV was made using the BrdU (5-bromo-2′-deoxyuridine) ELISA-based assay kit (Millipore, Corporation, MA, USA). For this test, 100 μL of the cells were plated and cultured at a concentration of 2 × 10^5 cell mL^{-1} in 96-well plates at 37 °C. Various UV-irradiation dose (1.8, 3.0, 6.0, 12.0 J cm^{-2}) were then used to treat each group. After the relevant incubation times (6, 24, and 48 h), the BrdU reagent were added to culture medium, with a final concentration of 3 μ mL^{-1}. Then the cells were incubated for 2 h. Then the cells were fixed with a fixative solution and the DNA was denatured in one-step by adding 200 μL well^{-1} of the fixative solution and incubation at room temperature for 30 min. After three-time washings, 100 μL well^{-1} of anti-BrdU monoclonal antibody was added to bind to the BrdU in the newly synthesized cellular DNA. Then, peroxidase-labeled goat anti-Mouse IgG was added to make immune complexes detectable after 30 min incubation with 100 μL well^{-1} of TMB peroxidase substrate at room temperature in the dark. Finally, the reaction product was quantified by the addition of 2 N hydrochloric acid stop solution and measuring the absorbance using a microplate reader (Varioskan Flash) at a wavelength of 525 nm. HBSS treated cells were used as negative controls.

The pH-Dependent ζ-Potential Changes of the NPs: The NPs solutions were diluted to 25 μg mL^{-1} using PBS of pH 5.0, 6.0, 6.8, 7.4, and 8.0, respectively, and then incubated at 37 °C. Then the NPs solutions were measured by a Zetasizer Nano ZS. Each measurement was performed for 30 runs, and the results were processed with DTS software.

Protein Adsorption of the NPs: The NPs were incubated with 10% human serum at pH 6.8 or 7.4, with the final concentration of NPs at1 mg mL^{-1}. After incubation at 37 °C for 1 h, 200 μL of each sample were centrifuged at 13 000 × *g* for 5 min to precipitate the protein adsorbed NPs. The protein concentration of supernatant was determined using UV-Vis spectroscopy (UV-1600 PB spectrophotometer, VWR) by measuring the maximal absorbance at 280 nm wavelength. Then, the adsorbed proteins on the NPs were calculated against a standard calibration curve of the proteins.

Drug Loading Degree: The loading degree of SFN was tested by an immersion method. Twenty-five micrograms of SFN-loaded UPBP NPs was suspended in 1 mL of DMF and stirred for 2 h. The supernatant then was obtained after centrifugation, and the concentration of SFN was determined by HPLC. For HPLC, the column used for SFN detection was C_{18} (4.6 × 100 × 3 mm, Gemini-Nx plus C18, Phenomenex, USA), and the mobile phase used consisted of 0.2% of trifluoroacetic acid (TFA; pH 2) and acetonitrile (42:58, v/v) with the flow rate of 1.0 mL min^{-1}. The temperature of the column and wavelength used for drug detection were 25 °C and 254 nm, respectively. The injected volume of the drug solution was 20 μL.

Drug Release of NPs Treated with UV Irradiation: The SFN-loaded UPBP NPs was dispersed in Milli-Q water first with the concentration of 50 μg mL^{-1}. Then the NP suspensions were irradiated for 1, 3, 5, and 20 min, respectively. The treated NPs were then mixed with equivalent volume of 20% human serum to obtain the 10% human serum NPs suspension, followed immediately by HPLC analysis. The method of HPLC analysis was the same as the part of drug loading degree.

Colloid Stability of UPBP NPs and Un-Bio@ZwS NPs: Hank's balanced salt solution—4-(2-hydroxyethyl)-1-piperazineethanesulfonic acid (HBSS–HEPES) buffer (pH 7.4) and 10% human serum (pH 7.4) were used to investigate the colloidal stability of the NPs with the NPs concentration of 25 μg mL^{-1}. Then the NPs solutions were measured by a Zetasizer Nano ZS. Each measurement was performed for 30 runs, and the results were processed with DTS software.

In Vitro Cytotoxicity: To evaluate the biosafety of the NPs, the viability of the MDA-MB-231 and NIH 3T3 fibroblast cells was assessed by measuring their ATP activity after exposure to the NPs. Hundred microliters of the cell suspensions in cell media at a concentration of 2 × 10^5 cells per mL were seeded in 96-well plates and allowed to attach overnight. After the removal of the cell media, the wells were washed twice with HBSS–HEPES buffer (pH 7.4), and then 100 μL of the tested NPs at the relevant concentrations was added. After incubation, the reagent assay (100 μL; CellTiter-Glo Luminescent Cell Viability Assay, Promega, USA) was added to each well to assess the ATP activity. The luminescence was measured using a Varioskan Flash (Thermo Fisher Scientific Inc., USA). Positive (1% Triton X-100) and negative (HBSS–HEPES buffer, pH 7.4) controls were also used and treated similarly as described above. At least three independent measurements were conducted for each experiment.

Confocal Imaging and FACS: For confocal fluorescence microscopy imaging, MDA-MB-231, 3T3 fibroblasts, and RAW 267.4 macrophages were seeded in eight-chamber slides (Nunc Lab-Tek II Chamber Slide System, Thermo Scientific, Inc., USA). For cell seeding, 200 μL of the cells suspension (2.5 × 10^4 cells mL^{-1}) was added to each chamber. After incubation for 24 h, the cells were washed twice with HBSS–HEPES buffer (pH 7.4). Two-hundred microliters of fluorescein isothiocyanate (FITC)–labeled NPs (10 μg mL^{-1}) was added to each chamber, and then the samples were incubated for 6 h. After that, the cells were washed with HBSS–HEPES buffer to remove noninteracting NPs. The cell membrane was stained with CellMask Deep Red (Life Technologies, USA) by incubating the cells at 37 °C for 3 min. Next, the cells were washed twice with the HBSS–HEPES buffer and fixed with 2.5% glutaraldehyde at room temperature for 20 min. Finally, the glutaraldehyde was washed away, and the cells were stored with 200 μL of HBSS–HEPES buffer (pH 7.4). The cells were observed under a confocal fluorescence microscope (Leica inverted SP5 II HCS A) using Ar (488 nm), HeNe (590 nm), and HeNe (633 nm) lasers. The images were analyzed using ImageJ 1.47v (National Institute of Health, USA).

For the cell uptake flow cytometry analysis, MB-231 cells, 3T3 fibroblasts, and RAW 267.4 macrophages were seeded in six-well plates (Corning Inc., Life Sciences, USA). For cell seeding, 2.5 mL of the cells suspension (2 × 10^5 cells per mL) were added to each well. The cell culturing process was based on the aforementioned method. After that, 1.5 mL of UPMFA NPs in HBSS–HEPES buffer with the concentration of 10 μg mL^{-1} were added to each well and then the samples were incubated for relevant time. After removing the NPs suspensions and washing twice with HBSS–HEPES buffer, the cells were harvested and treated with trypan blue to quench the fluorescence of NPs adhered on cell surface. Flow cytometry was performed with a LSR II flow cytometer (BD Biosciences, USA) with a laser excitation wavelength of 488 nm using a FACSDiva software. Ten thousand events were obtained for each sample. Relevant data were analyzed and plotted using FlowJo software (Tree Star Inc., USA). At least three independent measurements were conducted for each experiment.

Cell Growth Inhibition: The cell growth inhibition performance of the developed nanocomposites was also monitored by measuring the antiproliferation effect of the free SFN and SFN-loaded UPBP NPs using the same method explained above for the cellular toxicity studies. At least three independent measurements were conducted for each experiment.

Statistical Analysis: Quantitative data collected over multiple, independent experiments are presented as mean ± standard deviation (SD). At least three independent experiments ($n = 3$) were performed to obtain the described results. Statistical significance of the data was analyzed by a one-way analysis of variance (ANOVA) with Bonferroni post-hoc test (GraphPad Prism, GraphPad software Inc., CA, USA). The significance level was set at probabilities of $^*P < 0.05$, $^{**}P < 0.01$, and $^{***}P < 0.001$.

Supporting Information

Supporting Information is available from the Wiley Online Library or from the author.

Acknowledgements

F.Z. and L.K. contributed equally to this work. We acknowledge financial support from the Academy of Finland (decision no. 297580), Jane and Aatos Erkko Foundation (grant nos. 4704010), the Sigrid Jusélius Foundation (decision nos. 4704580), Orion Research Foundation, the University of Helsinki Research Funds, the Helsinki Institute of Life Science Funds, and the European Research Council under the European Union's Seventh Framework Programme (FP/2007-2013, Grant no. 310892). We thank the Electron Microscopy Unit and the Flow Cytometry Unit of the Institute of Biotechnology, University of Helsinki, for providing the necessary laboratory facilities and assistance.

Conflict of Interest

The authors declare no conflict of interest.

Keywords

photo-triggered zwitterization, porous silicon nanoparticles, protein corona, sequential antifouling surface, targeting delivery

Received: February 6, 2018
Revised: March 12, 2018
Published online: April 23, 2018

[1] D. Peer, J. M. Karp, S. Hong, O. C. Farokhzad, R. Margalit, R. Langer, *Nat. Nanotechnol.* **2007**, *2*, 751.
[2] C. J. Kearney, D. J. Mooney, *Nat. Mater.* **2013**, *12*, 1004.
[3] J. Shi, P. W. Kantoff, R. Wooster, O. C. Farokhzad, *Nat. Rev. Cancer* **2017**, *17*, 20.
[4] S. Tenzer, D. Docter, J. Kuharev, A. Musyanovych, V. Fetz, R. Hecht, F. Schlenk, D. Fischer, K. Kiouptsi, C. Reinhardt, K. Landfester, H. Schild, M. Maskos, S. K. Knauer, R. H. Stauber, *Nat. Nanotechnol.* **2013**, *8*, 772.

[5] F. Chen, G. Wang, J. I. Griffin, B. Brenneman, N. K. Banda, V. M. Holers, D. S. Backos, L. Wu, S. M. Moghimi, D. Simberg, *Nat. Nanotechnol.* **2017**, *12*, 387.
[6] M. P. Monopoli, C. Aberg, A. Salvati, K. A. Dawson, *Nat. Nanotechnol.* **2012**, *7*, 779.
[7] G. M. Mortimer, N. J. Butcher, A. W. Musumeci, Z. J. Deng, D. J. Martin, R. F. Minchin, *ACS Nano* **2014**, *8*, 3357.
[8] V. R. Devadasu, V. Bhardwaj, M. N. V. R. Kumar, *Chem. Rev.* **2013**, *113*, 1686.
[9] A. Salvati, A. S. Pitek, M. P. Monopoli, K. Prapainop, F. B. Bombelli, D. R. Hristov, P. M. Kelly, C. Aberg, E. Mahon, K. A. Dawson, *Nat. Nanotechnol.* **2013**, *8*, 137.
[10] H. C. Fischer, L. Liu, K. S. Pang, W. C. W. Chan, *Adv. Func. Mater.* **2006**, *16*, 1299.
[11] J. E. Dahlman, K. J. Kauffman, Y. Xing, T. E. Shaw, F. F. Mir, C. C. Dlott, R. Langer, D. G. Anderson, E. T. Wang, *Proc. Natl. Acad. Sci. U.S.A* **2017**, *114*, 2060.
[12] K. A. Whitehead, J. Matthews, P. H. Chang, F. Niroui, J. R. Dorkin, M. Severgnini, D. G. Anderson, *ACS Nano* **2012**, *6*, 6922.
[13] T. Dvir, M. R. Banghart, B. P. Timko, R. Langer, D. S. Kohane, *Nano Lett.* **2010**, *10*, 250.
[14] Y. Yang, J. Liu, X. Sun, L. Feng, W. Zhu, Z. Liu, M. Chen, *Nano Res.* **2016**, *9*, 139.
[15] Y.-Y. Yuan, C.-Q. Mao, X.-J. Du, J.-Z. Du, F. Wang, J. Wang, *Adv. Mater.* **2012**, *24*, 5476.
[16] T. Mizuhara, K. Saha, D. F. Moyano, C. S. Kim, B. Yan, Y.-K. Kim, V. M. Rotello, *Angew. Chem. Int. Ed.* **2015**, *54*, 6567.
[17] Z. S. Al-Ahmady, W. T. Al-Jamal, J. V. Bossche, T. T. Bui, A. F. Drake, A. J. Mason, K. Kostarelos, *ACS Nano* **2012**, *6*, 9335.
[18] D. K. Schach, W. Rock, J. Franz, M. Bonn, S. H. Parekh, T. Weidner, *J. Am. Chem. Soc.* **2015**, *137*, 12199.
[19] K. P. García, K. Zarschler, L. Barbaro, J. A. Barreto, W. O'Malley, L. Spiccia, H. Stephan, B. Graham, *Small* **2014**, *10*, 2516.
[20] H. S. Choi, B. I. Ipe, P. Misra, J. H. Lee, M. G. Bawendi, J. V. Frangioni, *Nano Lett.* **2009**, *9*, 2354.
[21] C. D. Walkey, J. B. Olsen, H. Guo, A. Emili, W. C. W. Chan, *J. Am. Chem. Soc.* **2012**, *134*, 2139.
[22] V. Mirshafiee, M. Mahmoudi, K. Lou, J. Cheng, M. L. Kraft, *Chem. Comm.* **2013**, *49*, 2557.
[23] X. Cheng, X. Tian, A. Wu, J. Li, J. Tian, Y. Chong, Z. Chai, Y. Zhao, C. Chen, C. Ge, *ACS Appl. Mater. Interfaces* **2015**, *7*, 20568.
[24] J. Su, F. Chen, V. L. Cryns, P. B. Messersmith, *J. Am. Chem. Soc.* **2011**, *133*, 11850.
[25] W. X. Ren, J. Han, S. Uhm, Y. J. Jang, C. Kang, J.-H. Kim, J. S. Kim, *Chem. Comm.* **2015**, *51*, 10403.
[26] S. Bhuniya, S. Maiti, E.-J. Kim, H. Lee, J. L. Sessler, K. S. Hong, J. S. Kim, *Angew. Chem. Int. Ed.* **2014**, *53*, 4469.
[27] H. Zhao, E. S. Sterner, E. B. Coughlin, P. Theato, *Macromolecules* **2012**, *45*, 1723.
[28] I. Tomatsu, K. Peng, A. Kros, *Adv. Drug Deliv. Rev.* **2011**, *63*, 1257.
[29] L. Kong, S. H. C. Askes, S. Bonnet, A. Kros, F. Campbell, *Angew. Chem. Int. Ed.* **2016**, *55*, 1396.
[30] K. Peng, I. Tomatsu, B. van den Broek, C. Cui, A. V. Korobko, J. van Noort, A. H. Meijer, H. P. Spaink, A. Kros, *Soft Matter* **2011**, *7*, 4881.
[31] M. K. G. Jayakumar, N. M. Idris, Y. Zhang, *Proc. Natl. Acad. Sci. U.S.A* **2012**, *109*, 8483.
[32] F. Zhang, A. Correia, E. Mäkilä, W. Li, J. Salonen, J. J. Hirvonen, H. Zhang, H. A. Santos, *ACS Appl. Mater. Interfaces* **2017**, *9*, 10034.
[33] F. Fontana, M.-A, Shahbazi, D. Liu, H. Zhang, E. Mäkilä, J. Salonen, J. T. Hirvonen, H. A. Santos, *Adv. Mater.* **2017**, *29*, 1603239.
[34] C.-F. Wang, M. P. Sarparanta, E. M. Mäkilä, M. L. K. Hyvönen, P. M. Laakkonen, J. J. Salonen, J. T. Hirvonen, A. J. Airaksinen, H. A. Santos, *Biomaterials* **2015**, *48*, 108.
[35] D. P. Nair, M. Podgórski, S. Chatani, T. Gong, W. Xi, C. R. Fenoli, C. N. Bowman, *Chem. Mater.* **2014**, *26*, 724.
[36] L. Wofsy, S. Singer, *J. Biochem.* **1963**, *2*, 104.
[37] J. Nam, N. Won, J. Bang, H. Jin, J. Park, S. Jung, S. Jung, Y. Park, S. Kim, *Adv. Drug Deliv. Rev.***2013**, *65*, 622.
[38] S. Pasche, J. Vörös, H. J. Griesser, N. D. Spencer, M. Textor, *J. Phys. Chem. B* **2005**, *109*, 17545.
[39] K. M. Piafsky, O. Borga, *Clin. Pharmacol. Ther.* **1977**, *22*, 545.
[40] J. B. Schlenoff, *Langmuir* **2014**, *30*, 9625.
[41] J. G. Vineberg, E. S. Zuniga, A. Kamath, Y.-J. Chen, J. D. Seitz, I. Ojima, *J. Med. Chem.* **2014**, *57*, 5777.
[42] H. Gao, W. Shi, L. B. Freund, *Proc. Natl. Acad. Sci. U.S.A.* **2005**, *102*, 9469.
[43] S. Zhang, J. Li, G. Lykotrafitis, G. Bao, S. Suresh, *Adv. Mater.* **2009**, *21*, 419.
[44] N. Chuard, G. Gasparini, D. Moreau, S. Lörcher, C. Palivan, W. Meier, N. Sakai, S. Matile, *Angew. Chem. Int. Ed.* **2017**, *56*, 2947.
[45] H. H. Gustafson, D. Holt-Casper, D. W. Grainger, H. Ghandehari, *Nano Today* **2015**, *10*, 487.
[46] M. C. Villarroel, K. W. Pratz, L. Xu, J. J. Wright, B. D. Smith, M. A. Rudek, *Invest. New Drugs* **2012**, *30*, 2096.
[47] Y. Lu, J. Yang, E. Sega, *AAPS J.* **2006**, *8*, E466.
[48] A. J. Keefe, S. Jiang, *Nat. Chem.* **2012**, *4*, 59.
[49] L. M. Bimbo, M. Sarparanta, H. A. Santos, A. J. Airaksinen, E. Mäkilä, T. Laaksonen, L. Peltonen, V.-P. Lehto, J. Hirvonen, J. Salonen, *ACS Nano* **2010**, *4*, 3023.

